Shape and dielectric mismatch effects in semiconductor quantum dots

P. G. Bolcatto* and C. R. Proetto
Comisión Nacional de Energía Atómica, Centro Atómico Bariloche and Instituto Balseiro, 8400 Bariloche, Argentina
(Received 22 June 1998; revised manuscript received 21 January 1999)

The combined effect of shape and dielectric mismatch between dot and matrix on several electronic properties of semiconductor quantum dots have been studied. In particular, the electronic properties of spherical and cubic quantum dots that have been analyzed are the integrated density of states, the polarization self-energy corrections to single-particle energies, the doping with impurities, excitonic Coulomb energies, and Coulomb blockade energies. It has been found that, in spite of the highly nonhomogeneous polarized charge density induced at the boundaries of the cubic quantum dot, the electronic properties are essentially independent on the dot shape for all the range of dielectric mismatch. [S0163-1829(99)00119-8]

I. INTRODUCTION

Semiconductor quantum dots (QD) can be characterized as systems where the carriers (electrons, holes) are confined in the three spatial directions. An immediate and clear consequence of this confinement is that their electronic structure collapses to a series of discrete levels, contrary to the continuous density of states associated to bulk semiconductors, or to their higher dimensional relatives, such as quantum wells and quantum wires. Besides, this discrete level structure can only be filled by a finite number of particles, while in quantum wells and wires, because of the incomplete confinement, it is still possible to have a macroscopic occupation of the samples. Given these features, semiconductor quantum dots are also termed as artificial atoms or zero-dimensional systems.[1–3]

One issue whose importance increases as dimensions are reduced is the shape of these artificial structures: with only a few exceptions, most of the dot calculations assume a spherical shape, because the high symmetry allows analytical results in many cases. This is one issue that motivated the present work: To what extent are the QD properties dependent of the assumed shape for the QD? As a test we compare several properties, such as one-electron energies through their integrated density of states (IDOS) and polarization self-energy corrections, binding energy of arbitrarily located impurities, excitonic Coulomb interactions, and two-electron properties, of equal volume spherical and cubic quantum dots (SCD's and CQD's, respectively). While neither of the two shapes can be taken too seriously, approximately SQD's are believed to form when grown from a colloidal suspension;[4] on the other side, other growth procedures such as self-ordering mechanisms during epitaxy of lattice-mismatched materials (typically, InGaAs/GaAs) seem to give rise to QD's of pyramidal shape.[5] Finally, the twofold cleaved edge overgrowth technique of Wegscheider *et al.*[6] should form QD's close to a cubic shape at the intersection of three quantum wells. One additional reason to adopt the cubic geometry as an alternative to the spherical geometry is that calculations can be carried out rather easily, although not so easily as in the spherical geometry. Any other shape choice, besides these two, almost inevitably leads to nonseparable wave functions and accordingly to complicated two- or three-dimensional numerical calculations, even to solve the single-particle case.[7]

A second important issue in the physics of quantum dots are dielectric mismatch or image charge effects. Most of the time, quantum dots of a given semiconductor material are embedded in a matrix of a different semiconductor or glass material, whose dielectric properties are usually quite different as compared with the dot material. This dielectric mismatch at the QD interface has important consequences, as in the presence of charged particles inside the dot (electrons, holes, impurities, etc.) they induce superficial charges at the boundaries. These induced charges interact in turn with the particles, and as these interactions are of the same magnitude as the Coulomb interaction between the real particles, they should be taken into account from the beginning. While there already exists in the literature a vast number of theoretical papers devoted to this issue, in the specific case of quantum dots all of them assume the spherical geometry, where calculations can be done quite easily, almost analytically.[8] It is the aim of the present contribution to study the *combined* effect of both shape and dielectric confinement effects, which as far as we know has not been addressed previously.

All the calculations to be presented below are made using the so-called strong confinement approximation,[9] whose validity is restricted to dot sizes smaller than the effective Bohr radius of the semiconductor in question. In practical terms, and this will be discussed in detail below, it amounts to treating electron-hole, electron-electron, and hole-hole Coulomb interactions as perturbations from the single-particle kinetic-energy contributions.

The rest of the paper is organized as follows: We give in Sec. II all the necessary theoretical results and general background which will be used in the following sections; Sec. III is devoted to the results for one-particle energies, polarization self-energy corrections, impurity properties, and exciton and two-electron features, while in Sec. IV we give the conclusions. All the detailed derivation of the results presented in the main body of the paper (mainly Sec. II) are given in the appendix.

II. THEORY

The aim of this work is focused on the study of the dependence of several electronic properties of quantum dots on

the geometry and dielectric mismatch between dot and matrix. Within the envelope wave-function approach to the effective-mass approximation,[10] the relevant Hamiltonian for an electron-hole pair confined by infinite barriers inside a QD with dielectric constant ε_1 embedded in a matrix with dielectric constant ε_2 is given by

$$H(\mathbf{r}_e,\mathbf{r}_h)=H_e(\mathbf{r}_e)+H_h(\mathbf{r}_h)+V_c(\mathbf{r}_e,\mathbf{r}_h), \tag{1}$$

where

$$H_e(\mathbf{r}_e)=-\frac{\hbar^2}{2m_e^*}\nabla_e^2+V_s(\mathbf{r}_e), \tag{2}$$

and

$$H_h(\mathbf{r}_h)=-\frac{\hbar^2}{2m_h^*}\nabla_h^2+V_s(\mathbf{r}_h). \tag{3}$$

In H_e (H_h) the first term corresponds to the electron (hole) kinetic energy, the second one to the self-energy which arises as result of the interaction between the electron (hole) and the surface charge density induced by itself at the boundary. Besides, $m_e^*(m_h^*)$ denotes the electron (hole) effective mass of the semiconductor well-acting material. The last term V_c is the generalized Coulomb interaction (including the interaction with the induced charges, see below) between the electron and hole. The Hamiltonian given by Eq. (1) may also be used to study the problem of doping quantum dots: taking the limit $m_h^*\to\infty$, the hole becomes a classical particle and it can be assimilated to a static donor impurity which can be located inside or outside the quantum dot.

The expressions for $V_c(\mathbf{r}_e,\mathbf{r}_h)$, $V_s(\mathbf{r}_e)$, and $V_s(\mathbf{r}_h)$ can be obtained from basic electrostatics as[11]

$$V_c(\mathbf{r}_e,\mathbf{r}_h)=-\frac{e_0^2}{\varepsilon_1}\frac{1}{|\mathbf{r}_e-\mathbf{r}_h|}-\frac{e_0}{\varepsilon_1}\int d\mathbf{r}'\frac{\sigma_{pol}(\mathbf{r}',\mathbf{r}_h)}{|\mathbf{r}_e-\mathbf{r}'|}, \tag{4}$$

and

$$V_s(\mathbf{r})=\frac{e_0^2}{2\varepsilon_1}\int d\mathbf{r}'\frac{\sigma_{pol}(\mathbf{r}',\mathbf{r})}{|\mathbf{r}-\mathbf{r}'|}, \tag{5}$$

where $-e_0$ is the electron charge and σ_{pol} is the polarized charge density at the dot boundaries induced by the hole. The energy potential $V_c(\mathbf{r}_e,\mathbf{r}_h)$ is invariant under the exchange of electron and hole coordinates. When there is not dielectric mismatch in the system ($\varepsilon_1=\varepsilon_2$), V_c is reduced to the bare Coulomb interaction $V_c(\mathbf{r}_e,\mathbf{r}_h)=-e_0^2/\varepsilon_1|\mathbf{r}_e-\mathbf{r}_h|$ and $V_s(\mathbf{r})=0$. The expressions (4) and (5) are dependent of the QD's geometry, and explicit expressions for them are given below.

For spherical quantum dots (SQD) of radius R, we will use the corresponding expressions given in Ref. 12:

$$V_c(\mathbf{r}_e,\mathbf{r}_h)=-\frac{e_0^2}{\varepsilon_1 R}\sum_{l=0}^{\infty}P_l(\cos\gamma)\times\left[\Theta_{(1-\bar{r}_h)}\left(\frac{\bar{r}_<^l}{\bar{r}_>^{l+1}}+\frac{(\varepsilon_r-1)(l+1)}{(\varepsilon_r+1)l+1}\bar{r}_<^l\bar{r}_>^l\right)+\Theta_{(\bar{r}_h-1)}\left(\frac{\varepsilon_r(2l+1)}{(\varepsilon_r+1)l+1}\frac{\bar{r}_e^l}{\bar{r}_h^{l+1}}\right)\right], \tag{6}$$

and

$$V_s(\mathbf{r})=\frac{e_0^2}{2\varepsilon_1 R}\sum_{l=0}^{\infty}\frac{(\varepsilon_r-1)(l+1)}{(\varepsilon_r+1)l+1}\bar{r}^{2l}. \tag{7}$$

In Eqs. (6) and (7), $P_l(\cos\gamma)$ are the Legendre polynomials of order l, γ the angle between electron and hole (measured from the origin at the dot center), $\bar{r}_<(\bar{r}_>)$ the smallest (greatest) between $\bar{r}_e$ and $\bar{r}_h$, $\Theta(x)$ the step function, and $\varepsilon_r=\varepsilon_1/\varepsilon_2$ the dielectric contrast. All distances are measured in units of the dot radius R, that is $\bar{r}=r/R$. While the second term in the right-hand side of Eq. (6), corresponding to the hole outside the QD, never contributes in our infinite barrier approximation for the exciton problem, it gives a nonzero contribution even in this limit for the impurity problem, in which case the hole coordinate is assimilated to the impurity coordinate, which can be located outside the QD.

On the other side, the corresponding expressions for a cubic quantum dot (CQD) of side $2Q$, which are derived in detail in the appendix, can be approximated by

$$V_c(\mathbf{r}_e,\mathbf{r}_h)=-\frac{e_0^2}{\varepsilon_1 Q}\left[\frac{1}{\sqrt{\pi}}\int_0^\infty\frac{dt}{\sqrt{t}}\phi(\bar{x}_e,\bar{x}_h,t)\times\phi(\bar{y}_e,\bar{y}_h,t)\phi(\bar{z}_e,\bar{z}_h,t)+f(\mathbf{r}_e,\mathbf{r}_h)\right], \tag{8}$$

and

$$V_s(\mathbf{r})=\frac{e_0^2}{2\varepsilon_1 Q}\left[\frac{1}{\sqrt{\pi}}\int_0^\infty\frac{dt}{\sqrt{t}}\phi'_{(\bar{x},\bar{x},t)}\phi'_{(\bar{y},\bar{y},t)}\phi'_{(\bar{z},\bar{z},t)}+f_{(\mathbf{r})}\right], \tag{9}$$

where we have defined the ϕ functions as ($\varrho\equiv x,y,z$),

$$\phi_{(\bar{\varrho}_e,\bar{\varrho}_h,t)}=\Theta_{(1-\bar{\varrho}_h)}\sum_{l=-\infty}^{\infty}\xi^{|l|}e^{-t[\bar{\varrho}_e-2l-(-1)^l\bar{\varrho}_h]^2}+\Theta_{(\bar{\varrho}_h-1)}\frac{2\varepsilon_r}{(\varepsilon_r+1)}\sum_{l=0}^{\infty}\xi^{|l|}e^{-t[\bar{\varrho}_e-(-1)^l(2l+\bar{\varrho}_h)]^2} \tag{10}$$

with $|\bar{\varrho}_e|\leqslant 1$ and $\xi=(\varepsilon_r-1)/(\varepsilon_r+1)$. In the equations above all the distances are measured in units of the half edge of the dot Q, that is, $\bar{\varrho}=\varrho/Q$. $f(\mathbf{r}_e,\mathbf{r}_h)$ is a correction function which guarantees that Eqs. (8) and (9) are equal to Eqs. (4) and (5). In most of the cases $f(\mathbf{r}_e,\mathbf{r}_h)$ is essentially a constant (i.e., independent of coordinates) approximately equal to $f(\mathbf{r}_e,\mathbf{r}_h)\equiv C\simeq 0.89\varepsilon_r(\varepsilon_r-1)$. Only when the impu-

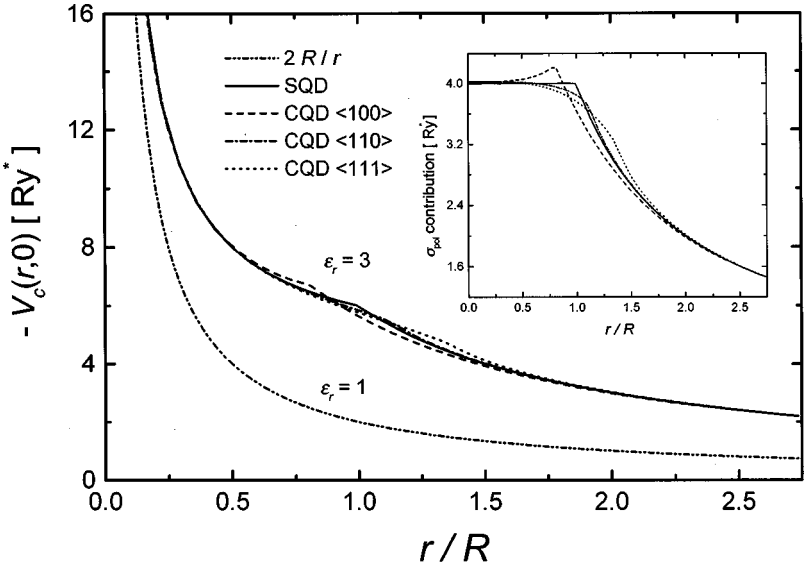

FIG. 1. Absolute value of the potential energy $-V_c(\mathbf{r},0)$ as a function of the distance from the dot center [Eq. (4)]. Full line, spherical geometry; dashed line, cubic geometry with $\mathbf{r}$ running along the $\langle 100\rangle$ directions; dashed-dotted line, cubic geometry with $\mathbf{r}$ running along the $\langle 110\rangle$ directions; dotted line, cubic geometry with $\mathbf{r}$ running along the $\langle 111\rangle$ directions. The lower isolated curve corresponds to the bare Coulomb interaction, equal to $2/\bar{r}$ in units of Ry*. The inset shows the contribution to the potential energy due to polarized charges at the dot boundary.

rity is outside the dot, $f(\mathbf{r}_e,\mathbf{r}_h)$ is dependent of $\mathbf{r}_h$, because in this case the potential energy has to tend towards its asymptotic expression $e_0^2/\varepsilon_2 r_h$. In Eq. (9) the real charge contribution must be excluded (this is the meaning of the primes in the ϕ functions).

In Fig. 1 we plot the absolute value of the potential energy $V_c(\mathbf{r}_e,\mathbf{r}_h)$ for the particular case $\mathbf{r}_h=0$ and $\mathbf{r}_e\equiv\mathbf{r}$ taking values inside and outside the dot. The lower curve corresponds to the absence of dielectric mismatch at the dot boundary, in which case only the first term in Eq. (4) contributes and $-V_c(\mathbf{r},0)$ reduces to $2/\bar{r}$ (in effective units). The upper set of curves correspond to a typical dielectric mismatch $\varepsilon_r=3$, the difference between both sets of curves being the polarization contribution given by the second term in Eq. (4). The inset displays precisely only this contribution to the potential energy. As far as we know, this is the first time that the potential energy of a cubic dot with dielectric contrast is presented. The first thing to note is the close similarity between the results for spherical and cubic dots. While just a simple curve is enough for the spherical dot, corresponding to r moving along an arbitrary radial direction, for the cubic case in principle each radial direction gives a different result. In consequence, for the cubic dot we have plotted the potential along three representative directions. The cusp in the potential energy as the coordinate moves along a $\langle 100\rangle$ direction is easily explained as in this case the particle is moving towards the center of one of the cube faces, which is the surface closest point to the dot center, and consequently where the maximum of the induced charge lies. This effect is absent when the particle is moving along a $\langle 110\rangle$ or $\langle 111\rangle$ directions, as the cube edge and vertex are places with small values for the induced charge. Indeed, $\sigma_{pol}(\mathbf{r},0)$ takes its minimum value at $\mathbf{r}=(Q,Q,Q)$ (and equivalents). Taken that all dot properties in which we are interested are essentially integrals of $V_c(\mathbf{r}_e,\mathbf{r}_h)$ weighted with the electron and/or hole wave functions, and from the quite similar results obtained for V_c in cubic and spherical environments, it is tempting to conclude also quite similar results for the electronic properties. The detailed calculations of the following sections are devoted to the quantitative confirmation of this qualitative expectation.

The electronic properties that we are interested in analyzing are: (i) the single-particle energies and their associated density of states (DOS), (ii) the polarization self-energy corrections, (iii) the Coulomb energy between an electron and a donor impurity arbitrarily located inside or outside the dot, as well as the dependence with the dielectric constant ratio ε_r, (iv) the exciton Coulomb energy between an electron-hole pair, and (v) the Coulomb blockade energy.

Furthermore, we adopt the so-called strong-confinement approximation (SCA) in solving the exciton Hamiltonian given by Eq. (1). This approximation is based in the simple fact that as the dot size decreases, the kinetic energy of both electron and hole scales as R^{-2} or Q^{-2} [see Eqs. (17) and (19)], while self-energy and Coulomb interactions scale as R^{-1} or Q^{-1} [see Eqs. (6)–(9)]. This means that in the small dot size limit (the length scale corresponding to the exciton Bohr radius) the latter becomes smaller than the former, and can be treated by perturbation theory. Accordingly, in this strong-confinement limit, the zero-order exciton Hamiltonian is reduced to the kinetic-energy terms[9]

$$H^{(0)}(\mathbf{r}_e,\mathbf{r}_h)=-\frac{\hbar^2}{2m_e^*}\nabla_e^2-\frac{\hbar^2}{2m_h^*}\nabla_h^2. \tag{11}$$

Consistently with this perturbative approach, the zero-order wave functions of $H^{(0)}$ can be expressed as a simple product of functions for the electron and hole, respectively, by $\Psi(\mathbf{r}_e,\mathbf{r}_h)=\psi(\mathbf{r}_e)\varphi(\mathbf{r}_h)$. In this way, the resolution of $H^{(0)}$ is decoupled in two equivalent problems:

$$-\frac{\hbar^2}{2m_e^*}\nabla_e^2\psi(\mathbf{r}_e)=E^{(0)}\psi(\mathbf{r}_e), \tag{12}$$

and

$$-\frac{\hbar^2}{2m_h^*}\nabla_h^2\varphi(\mathbf{r}_h)=E^{(0)}\varphi(\mathbf{r}_h), \tag{13}$$

with the hard-wall boundary condition that both $\psi(\mathbf{r}_e)$ and $\varphi(\mathbf{r}_h)$ should vanish on the boundaries of the QD.

Within this strong-confinement limit, the calculation of coulombic attraction and the self-polarization energies associated with $V_c(\mathbf{r}_e,\mathbf{r}_h)$, $V_s(\mathbf{r}_e)$, and $V_s(\mathbf{r}_h)$, respectively, is performed evaluating the corresponding average values using as wave functions the (zero-order) one-particle functions $\psi(\mathbf{r}_e)$ and $\varphi(\mathbf{r}_h)$.

$$\Sigma\equiv\int d\mathbf{r}\psi^*(\mathbf{r})V_s(\mathbf{r})\psi(\mathbf{r}), \tag{14}$$

$$E_{imp}(\mathbf{r}_i)\equiv-\int d\mathbf{r}_e\psi^*(\mathbf{r}_e)V_c(\mathbf{r}_e,\mathbf{r}_i)\psi(\mathbf{r}_e), \tag{15}$$

$$E_{Coul}\equiv-\int d\mathbf{r}_e d\mathbf{r}_h\psi^*_{(\mathbf{r}_e)}\varphi^*_{(\mathbf{r}_h)}V_{c(\mathbf{r}_e,\mathbf{r}_h)}\psi_{(\mathbf{r}_e)}\varphi_{(\mathbf{r}_h)}. \tag{16}$$

III. RESULTS

As a general rule, for the comparison of properties of SQD's and CQD's we will assume equal volume quantum dots, that is, $(2Q)^3=(4\pi/3)R^3$. Besides, for the graphical presentation of the results we will use the electron effective rydberg as unit of energy ($\mathrm{Ry}^*=m_e^*e_0^4/2\hbar^2\varepsilon_1$) and the size dot R as unit of length.

A. One-particle energies

The analysis of the one-particle energies could be performed either with Eqs. (12) or (13). For simplicity, we choose the electron case.

For a SQD, the solutions that satisfy the hard-wall boundary condition $\psi(\mathbf{r})=0$ are given by $\psi_{nlm}(\mathbf{r})=N_{nl}j_l(kr)Y_{lm}(\theta,\varphi)$, where $j_l(kr)$ are the spherical Bessel functions of the first kind of order l, $Y_{lm}(\theta,\varphi)$ are the spherical harmonics, and N_{nl} are the normalization constants. The single-particle energies are just the eigenvalues of the kinetic energy, given by

$$E_{nl}^{(0)}=\frac{\hbar^2}{2m_e^*}\frac{k_{nl}^2}{R^2}, \tag{17}$$

where k_{nl} ($n=1,2,3,\ldots$) are the ascending roots of the Bessel functions of order l. For a given value of l, the independence of equation above on the azimuthal quantum number m implies a degeneracy of $2l+1$ for each eigenvalue.

For CQD's, the normalized zero-order wave functions are

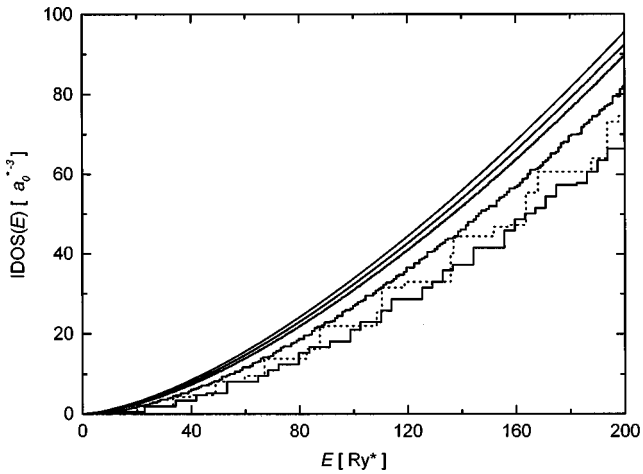

FIG. 2. Integrated density of states per unit volume for spherical quantum dots (dotted line) and cubic quantum dots of increasing size (full lines), as a function of energy. The top full line corresponds to the free-electron gas, which can be thought of as a quantum dot of infinite size.

$$\psi_{k_xk_yk_z}(\mathbf{r}_e)=\frac{1}{Q^{3/2}}\cos\left(\frac{\pi k_x\overline{x_e}}{2}-\alpha_x\right)\cos\left(\frac{\pi k_y\overline{y_e}}{2}-\alpha_y\right)\times\cos\left(\frac{\pi k_z\overline{z_e}}{2}-\alpha_z\right), \tag{18}$$

with $k_x,k_y,k_z=1,2,\ldots,$ and $\alpha_j=\pi/2(0)$ when k_j is even (odd), j being any of the three Cartesian components x,y,z. The corresponding energies are

$$E^{(0)}_{k_xk_yk_z}=\frac{\hbar^2}{2m_e^*}\left(\frac{\pi}{2Q}\right)^2(k_x^2+k_y^2+k_z^2). \tag{19}$$

The degeneracy of each eigenvalue in this case is given by the number of all possible combinations of k_x,k_y,k_z such that $k_x^2+k_y^2+k_z^2=$ same integer number.

We give in Fig. 2 the integrated density of states (IDOS) per unit volume for SQD's (dotted line, $\lambda=R/a_e^*=1$) and CQD's (full lines; from bottom to top: $\lambda=1,2,5,10,\infty$); they are defined as

$$\mathrm{IDOS}^{SQD}(E)=\frac{2}{V}\sum_{n,l}(2l+1)\Theta(E-E^{(0)}_{n,l}), \tag{20}$$

and

$$\mathrm{IDOS}^{CQD}(E)=\frac{2}{V}\sum_{k_x,k_y,k_z}\Theta(E-E^{(0)}_{k_xk_yk_z}), \tag{21}$$

V being the volume dot (assumed to be equal) and the factor of two comes from spin degeneracy. Physically, the IDOS gives the total number of states below a given energy E. Basically, the IDOS of equal size SQD's and CQD's have a similar behavior, with small differences due to the different symmetry of the two QD's: the IDOS for SQD is almost always above the IDOS for CQD, as a consequence of the greater degeneracy of the SQD eigenvalues, compared with the CQD ones. On the other side, the smaller degeneracy of the latter implies that the IDOS jumps more frequently than

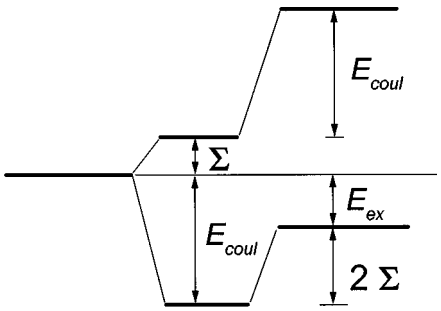

FIG. 3. Schematic view of the shift of the lowest conduction level due to the injection of one electron (Σ) or two electrons ($\Sigma + E_{Coul}$). E_{ex} represents the excitonic correction to the energy needed to create an electron-hole pair inside the quantum dot.

the IDOS for SQD. When calculated for a large enough number of eigenvalues, however, both effects compensate each other and the IDOS of SQD and CQD show no appreciable differences. The strong resemblance between both IDOS can be considered as a validation of our assumption of taking equal volume quantum dots as a criterion for their comparison. An interesting question to study is how the IDOS evolves when one moves to larger dot sizes. We provide the answer in the same Fig. 2, where we show the IDOS for CQD of increasing size (the IDOS of SQD's shows a similar behavior). The top full line corresponds to the IDOS per unit volume of the free electron gas, given by $\mathrm{IDOS}(E) = (1/3\pi^2)(2m_e^* E/\hbar^2)^{3/2}$; as expected, the IDOS for finite size QD's evolves towards the free-electron gas expression as the dot size increases. Note, however, that even for $\lambda = 10$ there are appreciable differences between both IDOS. It should be pointed out that we are allowed to move to large dot sizes $\lambda \gg 1$ where the SCA is not valid, as we are studying single-particle energies.

B. Polarization self-energy corrections

The single-particle energies studied above correspond to a situation where the particle (electron or hole) is inside a quantum dot whose dielectric properties are the same as that of the surrounding media. However, in the real situation, the surroundings of the quantum dot is a material media that can be polarized by the presence of the electric charge. This simple fact leads to a single-particle energy shift Σ due to the Coulomb interaction between the real and induced charges: an electron induces a bound surface charge density which in turn generates an electrostatic potential at the electron's position. A schematic diagram of this self-energy shift is shown in Fig. 3. The ground-state image charge contributions to the electron self-energy were first determined in Ref. 8 for SQD's, and given as

$$\Sigma^{SQD}(R) = \frac{e_0^2}{\varepsilon_1 R}\sum_{l=0}^{\infty}\frac{(\varepsilon_r-1)(l+1)}{(\varepsilon_r+1)l+1}\int_0^1 dx x^{2l}\sin^2(\pi x)$$

$$= \frac{e_0^2}{2\varepsilon_1 R}(\varepsilon_r-1) + \delta\Sigma(R), \tag{22}$$

where the first term on the right-hand side of the last equation is the $l=0$ contribution, while $\delta\Sigma$ corresponds to the remaining $l\neq 0$ contributions. When $\varepsilon_1+\varepsilon_2 \gg 1$, $\delta\Sigma$ may be approximated as[13]

$$\delta\Sigma(R) \cong 0.47\frac{e_0^2}{\varepsilon_1 R}\frac{(\varepsilon_r-1)}{(\varepsilon_r+1)}. \tag{23}$$

On the other side, according to Eq. (A11), the ground-state polarization self-energy corrections for CQD's are given by

$$\Sigma^{CQD}(Q) = \frac{e_0^2}{2\varepsilon_1 Q}\left\{\frac{1}{\sqrt{\pi}}\int_0^{\infty}\frac{dt}{\sqrt{t}}[I_1(t)]^3 + C\right\}, \tag{24}$$

with

$$I_1(t) = \sum_{l=-\infty}^{\infty}\xi^{|l|}\int_{-1}^{1} d\bar{x}\, e^{-t\{[1-(-1)^l]\bar{x}-2l\}^2}\cos^2\left(\frac{\pi\bar{x}}{2}\right). \tag{25}$$

In Eq. (24) a single term corresponding to the real charge contribution must be excluded.

We display in Fig. 5(a) a comparison of the self-energy corrections for SQD's and CQD's, corresponding to a dot size of $\lambda = 1$. The corrections are negative if $\varepsilon_r < 1$, and positive if $\varepsilon_r > 1$ (both being exactly zero in the absence of dielectric mismatch). This is due to the fact that the self-induced dot boundary charge is of the same (opposite) sign as the real charge if $\varepsilon_r > 1$ ($\varepsilon_r < 1$). In most of the dots fabricated to date $\varepsilon_r > 1$. It should be pointed out the importance of self-energy corrections as for a physically realizable dielectric ratio $\varepsilon_r \simeq 10$, Σ can reach values up to 10 Ry* which is quite comparable with the Coulomb energy E_{Coul}. On the other side, it is quite remarkable that in spite that the sharp boundaries of the cubic geometry induce a highly nonhomogeneous polarization charge density, the self-energy corrections are essentially shape independent.

C. Doping of a quantum dot

The study of the electronic properties of a donor impurity confined in a QD can be performed taking the limit $m_h^* \to \infty$ in Eq. (1). In this limit the hole plays the role of a positive donor impurity, and its coordinate becomes a parameter that can be treated as a classical variable. The relevant Hamiltonian includes only the first and third terms of Eq. (1). Defining as usual the impurity binding energy as the difference of the electron energy in the absence or presence of the positive ion, this magnitude becomes precisely given by Eq. (15); according to this definition, a positive value of $E_{imp}(\mathbf{r}_i)$ means that the configuration electron + impurity is more stable than the configuration with only the electron inside the QD. On-center binding energies of impurities in SQD's with dielectric mismatch were already studied by variational techniques in Ref. 14.

The corresponding analytical expressions of $E_{imp}(\mathbf{r}_i)$ for SQD's using the strong-confinement approximation were obtained in Ref. 12. For instance, for the ground state ($n=1, l=m=0$), this energy is

$$E_{imp}^{100}(r_i)=\frac{e_0^2}{\varepsilon_1 R}\left[\Theta(1-\bar{r}_i)\left(\varepsilon_r-\frac{\sin(2\pi\bar{r}_i)}{2\pi\bar{r}_i}+\mathrm{Cin}(2\pi)-\mathrm{Cin}(2\pi\bar{r}_i)\right)+\Theta(\bar{r}_i-1)\varepsilon_r/\bar{r}_i\right], \tag{26}$$

where $\bar{r}_i \equiv r_i/R$ is the impurity position inside ($\bar{r}_i 1 \leqslant$) or outside ($\bar{r}_i \geqslant 1$) the QD and Cin is the cosine integral function.[15] The superscripts denote the value of the quantum numbers *n*, *l*, and *m* of the zero-order spherical wave functions, respectively. Further analytical expressions for the *p*-like states ($l=1, m=0,\pm 1$) and numerical results for the ten zero-order lowest states are also provided in Ref. 12.

On the other hand, in the appendix the general expressions for this impurity binding energy in CQD's are derived. The zero-order ground state in a cubic box occurs when the three quantum numbers k_j are equal to 1, and then the first-order electron-impurity Coulomb energy is given by [see Eq. (A14)]

$$E_{imp}^{111}(\mathbf{r}_i)=\frac{e_0^2}{\varepsilon_1 Q}\left(\frac{1}{\sqrt{\pi}}\int_0^\infty \frac{dt}{\sqrt{t}} J_{11}(\bar{x}_i,t)\times J_{11}(\bar{y}_i,t)J_{11}(\bar{z}_i,t)+C(\mathbf{r}_i)\right), \tag{27}$$

where $(\bar{x}_i,\bar{y}_i,\bar{z}_i)=(x_i,y_i,z_i)/Q$, and

$$J_{11}(\bar{x}_i,t)=\int_{-1}^{1} d\bar{x}_e \cos^2(\pi\bar{x}_e/2)\,\phi(\bar{x}_e,\bar{x}_i,t). \tag{28}$$

Equations (26) and (27) are explicit expressions for the ground-state binding energies of arbitrarily located donor impurities in spherical and cubic dots, respectively. Both include dielectric mismatch effects at the dot boundaries. Clearly, the spherical geometry results in a much simpler expression, as compared with the cubic symmetry. It is important to realize, however, that all the size dependence in both expressions is identical, being contained in the prefactor that goes like R^{-1}or Q^{-1}.

A plot of $E_{imp}^{100}(r_i)$ and $E_{imp}^{111}(\mathbf{r}_i)$ as a function of $\bar{r}_i$ is given in Fig. 4 for SQD and CQD, respectively. Without loss of generality, we have chosen the *z* axis for the impurity displacements in SQD's. For the CQD case, three different representative directions ($\langle 100\rangle$, $\langle 110\rangle$, and $\langle 111\rangle$) were selected for the displacement of the impurity. The lower set of curves correspond to $\varepsilon_r=1$ (no dielectric mismatch between dot and matrix), which could apply to GaAs/Al_xGa_{1-x}As quantum dots, while the upper set of curves correspond to $\varepsilon_r=3$, which could apply to Si/*a*-SiO_2 quantum dots.[16]

Concentrating first in the results for $\varepsilon_r=1$, we obtain small differences between SQD's and CQD's, which decrease as the impurity moves towards the dot boundary. For instance, when the impurity is at the origin, the ratio $E_{imp}^{100}(0)/E_{imp}^{111}(0)$ is approximately 1.06, being the small differences mainly due to the fact that the cubic ground-state function is more concentrated around of the origin than the spherical one. For $\bar{r}_i \gtrsim 0.5$ binding energies for both geometries become essentially indistinguishable. For $\bar{r}_i \gg 1$ all the curves converge asymptotically to the expression $e_0^2/\varepsilon_2 r_i$, corresponding to the Coulomb interaction between two non-overlapping charge distributions in the ε_2 media: the point impurity and the spherically symmetric electronic density. The fact that this value is also reached for the cubic geometry is a good check on the accuracy of our calculations. The ground-state binding energy for CQD's shows no dependence on the direction in which the impurity is displaced, the results for the three analyzed directions essentially falling on the same curve. This is related to the fact that the electron ground-state wave function is the product of three identical factors along the *x*,*y*, and *z* directions [see Eq. (18)]. Accordingly, the total wave function results in an approximate spherical symmetry, which gives rise to a quite weak directional dependence. The remaining curves in Fig. 4 are the same as the four in the lower set but with a dielectric mismatch $\varepsilon_r=3$. The results for SQD's, already discussed in Ref. 12, show that the binding energy is an increasing function of the dielectric mismatch ($\varepsilon_r>1$), resulting in an enhancement of about 100% for this particular case ($\varepsilon_r=3$). The physics behind this dielectric enhancement is quite simple: The electron interacts *both* with the positive impurity and its induced charge. If $\varepsilon_r>1$ the impurity induced charge is also positive, resulting in an increased binding energy. Similar results are obtained for CQD, although a discernible difference can be observed as the impurity moves along different directions. The slope discontinuity in the curves with $\varepsilon_r=3$ is due to the boundary dielectric mismatch, which reflects in turn in a slope discontinuity of the corresponding potentials of Fig. 1. The kink occurs when the impurity moves out of the dot, that is, $\bar{r}_i=1$ for SQD but $\bar{r}_i \cong 0.81, 1.14$, and 1.40 for CQD and impurity displacements along the $\langle 100\rangle$, $\langle 110\rangle$, and $\langle 111\rangle$ directions, respectively. This difference in the distance from the dot center to dot

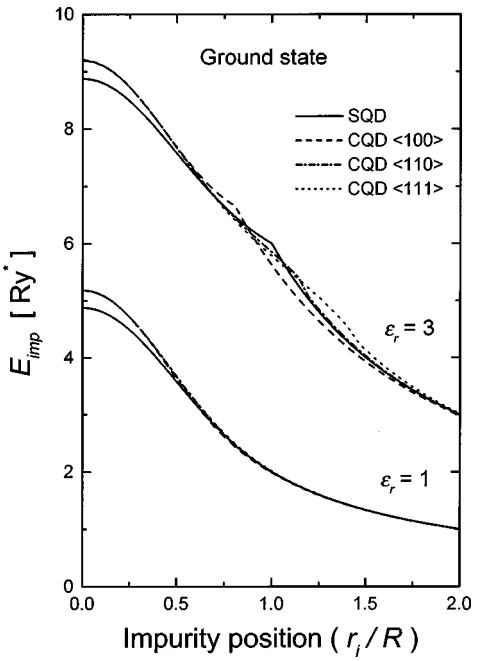

FIG. 4. Ground-state binding energy of impurities as a function of impurity position. Full lines correspond to spherical quantum dots, all the remaining lines correspond to cubic quantum dots. Dot size $\lambda = R/a_e^* = 1$.

boundary along the three directions breaks also the quasidegeneracy of the associated CQD binding energies, as the decay with impurity position is faster when the impurity moves out of the dot. It is also interesting that the binding energy depends strongly on the impurity position: for example, moving the impurity from center to boundary, the decrease in binding energy amounts to approximately 35%.

We have also analyzed the binding energy of the first- and second-excited states of CQD's (not shown). One important difference with respect to the ground-state results is that in this case the binding energy displays a nonmonotonic dependence on the impurity coordinate $\bar{r}_i$. As in the SQD's case, this is due to the fact that these excited states have a node in its charge distribution at the dot center, where consequently the binding energy attains a low value, and then presents a maximum value at same distance from the dot center. The dielectric enhancement effects are similar as to the ground-state case.

D. Exciton Coulomb energy

We will analyze in this section the shape and dielectric mismatch effects on the exciton Coulomb energy. This energy is defined as the correction to the size dependent band-gap energy needed to create an electron-hole pair inside the quantum dot. Then, this excitonic energy should include, besides the generalized Coulomb interaction between the negative and positive charges, the corresponding polarization self-energies of the electron and the hole (see Fig. 3). Within the strong-confinement approximation, the normalized ground-state exciton wave function for a SQD confined by infinite barriers is given by

$$\Psi_{ex}^{SQD}(\mathbf{r}_e,\mathbf{r}_h)=\psi_{100}(\mathbf{r}_e)\varphi_{100}(\mathbf{r}_h)=\frac{\pi}{2R^3}\frac{\sin(\pi\bar{r}_e)}{(\pi\bar{r}_e)}\frac{\sin(\pi\bar{r}_h)}{(\pi\bar{r}_h)}. \tag{29}$$

Taking the expectation value of the exciton Hamiltonian given by Eq. (1) without the kinetic energy terms (which together with the semiconductor bulk band gap E_g results in the size-dependent single particle band gap) with $\Psi_{ex}^{SQD}(\mathbf{r}_e,\mathbf{r}_h)$ we obtain

$$E_{ex}^{SQD}(R)\equiv 2\Sigma^{SQD}(R)-E_{Coul}^{SQD}(R), \tag{30}$$

where $\Sigma^{SQD}(R)$ is given by Eq. (22) and E_{Coul}^{SQD} is obtained from Eq. (16) as

$$E_{Coul}^{SQD}(R)=\frac{e_0^2}{\varepsilon_1 R}\left(\varepsilon_r+1-\frac{\mathrm{Si}(2\pi)}{\pi}+\frac{\mathrm{Si}(4\pi)}{2\pi}\right). \tag{31}$$

It is interesting to note that all l between 0 and ∞ contributes to $\Sigma^{SQD}(R)$, while only the term $l=0$ of $V_c(\mathbf{r}_e,\mathbf{r}_h)$ gives a non-zero contribution to $E_{Coul}^{SQD}(R)$. Replacing Eqs. (22) and (31) in Eq. (30) we obtain

$$E_{ex}^{SQD}(R)=\frac{e_0^2}{\varepsilon_1 R}\left[2\,\delta\Sigma(R)-\left(2-\frac{\mathrm{Si}(2\pi)}{\pi}+\frac{\mathrm{Si}(4\pi)}{2\pi}\right)\right], \tag{32}$$

where $\delta\Sigma(R)$ is what remains after an almost complete cancellation of polarization effects included both in the self-energy and $E_{Coul}^{SQD}(R)$. In equations above, Si(x) is the sine integral function,[15] and $\delta\Sigma(R)$ is given by Eq. (23). In the absence of dielectric mismatch ($\varepsilon_r=1, \delta\Sigma^{SQD}\equiv 0$) we obtain the well-known result

$$E_{ex}^{SQD}(R)\cong -1.786\frac{e_0^2}{\varepsilon_1 R}, \tag{33}$$

first obtained by Brus.[8]

Similarly, the ground-state exciton wave function for a CQD as given in the SCA is

$$\Psi_{ex}^{CQD}(\mathbf{r}_e,\mathbf{r}_h)=\frac{1}{Q^3}\cos\left(\frac{\pi}{2}\bar{x}_e\right)\cos\left(\frac{\pi}{2}\bar{y}_e\right)\cos\left(\frac{\pi}{2}\bar{z}_e\right)\times\cos\left(\frac{\pi}{2}\bar{x}_h\right)\cos\left(\frac{\pi}{2}\bar{y}_h\right)\cos\left(\frac{\pi}{2}\bar{z}_h\right). \tag{34}$$

Taking again the expectation value of the exciton Hamiltonian without the kinetic-energy contributions, but using this time $\Psi_{ex}^{CQD}(\mathbf{r}_e,\mathbf{r}_h)$ we obtain for the size dependent exciton energy

$$E_{ex}^{CQD}(Q)\equiv 2\Sigma^{CQD}(Q)-E_{Coul}^{CQD}(Q), \tag{35}$$

where $\Sigma^{CQD}(Q)$ is given by Eq. (24) and $E_{Coul}^{CQD}(Q)$ is defined in Eq. (A21) of the appendix. Contrary to the case with spherical geometry, no obvious cancellation exists between these two terms. In the absence of dielectric mismatch $\Sigma^{CQD}(Q)\equiv 0$, and only the $l=0$ contribution from the sum in Eq. (A22) survives; in this limit, the size dependent exciton energy reduces to

$$E_{ex}^{CQD}(Q)\cong -1.52\frac{e_0^2}{\varepsilon_1 Q}\cong -1.89\frac{e_0^2}{\varepsilon_1 R}, \tag{36}$$

a result first obtained by Fishman, Romestain, and Vial.[17] The similarity of $E_{ex}^{SQD}(R)$ and $E_{ex}^{CQD}(Q)$ in absence of dielectric mismatch is quite remarkable, the difference being around 5%. Moreover, the comparison of dielectric mismatch effects on excitonic properties of SQD's and CQD's in Fig. 5(b), shows that this similarity remains for all the range of dielectric mismatch ratio. Open circles correspond to Eq. (32), open squares to Eq. (35), and the full line corresponds to replace the analytical approximation for $\delta\Sigma$ given by Eq. (23) in Eq. (22). We can observe that this simple analytical expression agrees fairly well with the calculation, showing the smooth dependence of the excitonic energy with ε_r.

The exciton Coulomb energy provides us with an additional check about the consistency of our calculational approach. Noting that the correction factor C included in Σ^{CQD} and E_{Coul}^{CQD} cancels exactly in Eq. (35), the excitonic energy should be the same if calculated with Eqs. (A3) or (A7) for the potential $\Phi(\mathbf{r}_1,\mathbf{r}_2)$. We have performed the comparison and found that the difference between both calculations is indistinguishable on the scale of Fig. 5(b).

E. Coulomb blockade

The last property that we will consider is the energy necessary to put a second electron inside the QD, when already there is one, both in the same spatial state (for instance, the ground state) but with opposite spin.[18] The injection of a

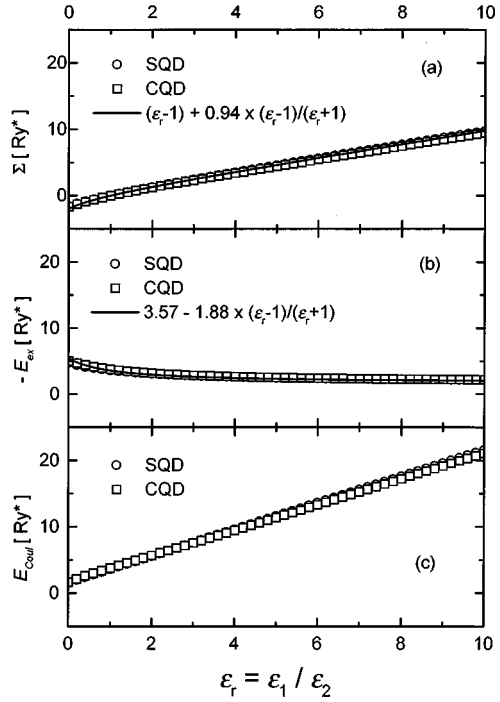

FIG. 5. Spherical quantum dot (open circles) and cubic quantum dot (open squares): (a) polarization self-energy corrections; (b) electron-hole excitonic Coulomb energies; and (c) Coulomb blockade energies as a function of the dielectric mismatch between dot and matrix. Dot size $\lambda = R/a_e^* = 1$.

second electron leads to an additional upwards shift (with respect to the injection of the first electron) given by the average repulsion with the other electron and its ''image charge.'' Accordingly, this energy is given by the magnitude E_{Coul} of Eq. (16). Explicit expressions for this energy in spherical and cubic quantum dots are provided by Eqs. (31) and (A21), respectively. In the context of electronic transport through quantum dots, this energy gives rise to the Coulomb blockade phenomena, as the QD conductance shown oscillations as a function of the applied gate voltage whose period is related to this energy.[19]

We present in Fig. 5(c) the dependence of this magnitude on the dielectric contrast, for both geometries. We have found once more a strong similarity between E_{Coul} for spherical and cubic geometries, both showing an almost identical linear increase with ε_r, as can be seen directly appreciated from Eq. (31).

IV. CONCLUSIONS

In this work we have studied the dependence of several electronic properties of semiconductor quantum dots on size, shape, and dielectric mismatch at the dot boundary. The properties studied included the one-particle energies, the polarization self-energy correction, the binding energy of impurities in quantum dots, excitonic Coulomb energies, and the so-called Coulomb blockade energies. As a model for the shape dependence, we have assumed two types of dots: spherical and cubic. The issue of the dependence of quantum dot properties on shape and dielectric mismatch at the dot boundary has already been studied in previous works, but including only one feature and not the other.

A first step for the study of the dot electronic properties within the framework of the strong-confinement approximation is the calculation of the generalized Coulomb potential, including the contribution of polarized charges at the dot boundaries. While this generalized Coulomb potential is well known in the spherical geometry, it is an important problem by itself in the cubic geometry. While we have found and presented the exact solution for this difficult problem, for the calculation of the electronic properties we have used a quite accurate approximation to the exact potential. The direct calculation with the exact potential is in principle feasible, but numerically quite demanding. Besides this technical difference, the generalized Coulomb potentials are quite similar for both geometries.

From a comparison of the results presented in Fig. 5, it is evident that the polarization self-energy correction Σ and the Coulomb energy E_{Coul} are strong (linear) functions of the dielectric contrast ε_r, while the excitonic energy shows a much weaker dependence. For the spherical geometry, this is due to an explicit partial cancellation between self-energy and Coulomb energies (which are of opposite signs if $\varepsilon_r > 1$); on the light of the results presented in Fig. 5(b), the same cancellation exists for the cubic symmetry, although in this case is far from being evident from the explicit analytical expressions. Physically, the weak dependance of the excitonic energy with the dielectric contrast reflects the charge neutrality of the exciton.

We have found that even in presence of dielectric mismatch, most of the electronic properties of quantum dots are weakly shape dependent, the important parameter being in this case the size (volume) of the dot. Typically, the difference between results for spherical or cubic quantum dots amounts to five percent or less. Accordingly, it seems reasonable to conclude that it will be quite difficult to obtain experimental information about the shape of quantum dots from measurements of excitonic properties. On the positive side, our work gives a solid base to the modeling of quantum dots as spherical particles, as far as excitonic properties are concerned.

ACKNOWLEDGMENTS

One of us (P.G.B.) wishes to acknowledge the financial support received from FOMEC No. 331, Universidad Nacional del Litoral. The authors are grateful to T. Takagahara for sending unpublished related material, and to Karen Hallberg for a careful reading of the manuscript.

APPENDIX: GENERAL EXPRESSIONS FOR THE POLARIZATION SELF-ENERGY, ELECTRON-IMPURITY POTENTIAL, AND EXCITONIC COULOMB ENERGY IN A CUBIC QUANTUM DOT

1. Electrostatic potential

In this appendix we give details on the derivation of the polarization contributions to the electron/hole polarization self-energy, the electron-donor impurity potential, and the electron-hole excitonic Coulomb interaction, for the case of a cubic quantum dot with dielectric mismatch at the boundaries.

We assume that the origin of the coordinate system coincides with the center of the cube and the boundaries are located at $x=\pm Q$, $y=\pm Q$, and $z=\pm Q$. Following Ref. 20, the electrostatic potential $\Phi(\mathbf{r}_1,\mathbf{r}_2)$ can be obtained using the image charge method. Thus, the potential at $\mathbf{r}_1=(x_1,y_1,z_1)$ inside the cubic dot when a charge of magnitude q (the source) is in the same region [i.e., $|x_2|<Q$, $|y_2|<Q$, and $|z_2|<Q$, being $\mathbf{r}_2=(x_2,y_2,z_2)$ the coordinate of the source charge] is given by

$$\Phi^{<}(\mathbf{r}_1,\mathbf{r}_2)=\frac{q}{\varepsilon_1 Q}\sum_{l,m,n=-\infty}^{\infty}\xi^{|l|+|m|+|n|}\times\frac{1}{[(\overline{x_1}-\overline{x_l})^2+(\overline{y_1}-\overline{y_m})^2+(\overline{z_1}-\overline{z_n})^2]^{1/2}},\tag{A1}$$

where $\overline{\mathbf{r}_i}=\mathbf{r}_i/Q$ and the parameter ξ is defined by $\xi=(\varepsilon_r-1)/(\varepsilon_r+1)$, being $\varepsilon_r=\varepsilon_1/\varepsilon_2$ the relation between the dielectric constant inside the dot (ε_1) and the surrounding media (ε_2). The coordinates of the infinite image charges are related with the coordinate of the source coordinate $\overline{\mathbf{r}_2}$ through $\overline{\mathbf{r}_{lmn}}\equiv(\overline{x_l},\overline{y_m},\overline{z_n})=[2l+(-1)^l\overline{x_2},2m+(-1)^m\overline{y_2},2n+(-1)^n\overline{z_2}]$. By using the following identity

$$\frac{1}{|\mathbf{r}-\mathbf{r}'|}=\frac{1}{\sqrt{\pi}}\int_0^{\infty}\frac{dt}{\sqrt{t}}e^{-t|\mathbf{r}-\mathbf{r}'|^2},\tag{A2}$$

Eq. (A1) can be written as an integral whose integrand is the product of three functions, each one of them for the three spacial directions. Namely,

$$\Phi^{<}(\mathbf{r}_1,\mathbf{r}_2)=\frac{q}{\varepsilon_1 Q}\frac{1}{\sqrt{\pi}}\int_0^{\infty}\frac{dt}{\sqrt{t}}\phi^{<}(\overline{x_1},\overline{x_2},t)\times\phi^{<}(\overline{y_1},\overline{y_2},t)\phi^{<}(\overline{z_1},\overline{z_2},t),\tag{A3}$$

where we have defined

$$\phi^{<}(\varrho_1,\varrho_2,t)=\sum_{l=-\infty}^{\infty}\xi^{|l|}e^{-t[\varrho_1-2l-(-1)^l\varrho_2]^2}\tag{A4}$$

with $\varrho\equiv x,y,z$, and $|\varrho_2|\leq 1$.

It could be checked that $\Phi^{<}(\mathbf{r}_1,\mathbf{r}_2)$ defined by Eq. (A3) [or Eq. (A1)] satisfies the electrostatic boundary conditions of our problem (the continuity of the electrostatic potential and the normal component of the displacement vector) at the dot boundary. For example, the boundary conditions at the face $x_1=Q(|y_1|\leq Q \text{and} |z_1|\leq Q)$ are satisfied if we define the potential $\Phi^{>}(\mathbf{r}_1,\mathbf{r}_2)$ for $x_1>Q(|y_1|\leq Q \text{and} |z_1|\leq Q)$ by replacing only the $\phi^{<}(\overline{x_1},\overline{x_2},t)$ function in Eq. (A3) by the following $\phi^{>}(\overline{x_1},\overline{x_2},t)$ function:

$$\phi^{>}(\overline{x_1},\overline{x_2},t)=\sum_{l=0}^{\infty}\frac{2\varepsilon_r}{(\varepsilon_r+1)}\xi^{|l|}e^{-t[\overline{x_1}+2l-(-1)^l\overline{x_2}]^2}.\tag{A5}$$

Proceeding in this way, it is easy to see that the boundary conditions $\Phi^{<}(\mathbf{r}_1,\mathbf{r}_2)|_{x_1=Q}=\Phi^{>}(\mathbf{r}_1,\mathbf{r}_2)|_{x_1=Q}$ and $\varepsilon_1(\partial/\partial x_1)\Phi^{<}(\mathbf{r}_1,\mathbf{r}_2)|_{x_1=Q}=\varepsilon_2(\partial/\partial x_1)\Phi^{>}(\mathbf{r}_1,\mathbf{r}_2)|_{x_1=Q}$ are fulfilled if $\phi^{<}(x_1,x_2)|_{x_1=Q}=\phi^{>}(x_1,x_2)|_{x_1=Q}$ and $\varepsilon_1(\partial/\partial x_1)\phi^{<}(x_1,x_2)|_{x_1=Q}=\varepsilon_2(\partial/\partial x_1)\phi^{>}(x_1,x_2)|_{x_1=Q}$. But the last two conditions are precisely the equations from where the one dimensional potentials are derived. The details of the calculation of these one-dimensional (quantum well) potentials can be obtained in Ref. 21. It should be emphasized that although the boundary conditions are satisfied separately for each of the three spacial directions, the potential is not a product of three one-dimensional potentials. In other words, the three spatial coordinates are mixed by the potential, as can be directly appreciated from Eq. (A3).

However, we must note that, unfortunately, the calculation of $\Phi^{<}(\mathbf{r}_1,\mathbf{r}_2)$ directly from Eq. (A3) is hampered by the following problem: we have found that in the case $\varepsilon_1/\varepsilon_2\gg 1$ (metallic dot limit), the potential increases quadratically with ε_1, instead of approaching a limiting value, as one should expect from physical grounds. On the other side, the opposite limit $\varepsilon_1/\varepsilon_2\ll 1$ (metallic matrix limit) is given correctly by the potential as defined by Eq. (A3). Basically, in this limit the potential is a decreasing function of $\mathbf{r}_1$ (for $\mathbf{r}_2=0$) and reaches exactly a null value when $\mathbf{r}_1$ reaches the dot boundary. Besides, and this is quite important for our calculation approach, also the spacial distribution of polarization charges at the dot boundaries are given correctly. Defining[11]

$$\sigma_{pol}(\mathbf{r}_1,\mathbf{r}_2)=-\frac{1}{4\pi}[(\varepsilon_2-1)\nabla\Phi^{>}(\mathbf{r}_1,\mathbf{r}_2)-(\varepsilon_1-1)\nabla\Phi^{<}(\mathbf{r}_1,\mathbf{r}_2)]\cdot\hat{\mathbf{n}},\tag{A6}$$

where $\hat{\mathbf{n}}$ is a unit vector normal to the surface separating media 1 from media 2 and pointing from 1 to 2, we have checked that $\sigma_{pol}(\mathbf{r}_1,\mathbf{r}_2)$ is given correctly. Qualitatively, taking for example $\mathbf{r}_2=0$, $\sigma_{pol}(\mathbf{r}_1,0)$ presents a maximum for $\mathbf{r}_1=(\pm Q,0,0)$ and equivalently along y and x directions, because these are the closest points to the source charge at the origin. From this maximum, $\sigma_{pol}(\mathbf{r}_1,0)$ decreases monotonically when $\mathbf{r}_1$ moves towards the cube edges and reach its minimum values at the cube vertices. Also the metallic dot limit is correctly given by $\sigma_{pol}(\mathbf{r}_1,\mathbf{r}_2)$: we have found that in the range $1\leq\varepsilon_1/\varepsilon_2\leq 10$,$\sigma_{pol}(\mathbf{r}_1,\mathbf{r}_2)$ evolves continuous from the smooth distribution with a maximum at the face cube center, to an essentially position independent constant value for $\varepsilon_1/\varepsilon_2=10$, as one should expect for a metalliclike particle. The definitive proof, however, about the correctness of $\sigma_{pol}(\mathbf{r}_1,\mathbf{r}_2)$ is that its integrated value on the six cube faces gives exactly $q(\varepsilon_1/\varepsilon_2-1)/\varepsilon_1$, as it should be according to properties of the polarization vector.

Thus an alternative way of calculating the electrostatic potential starting from the source charge q and the induced superficial charge density σ_{pol} is

$$\Phi(\mathbf{r}_1,\mathbf{r}_2)=\frac{q}{\varepsilon_1}\frac{1}{|\mathbf{r}_1-\mathbf{r}_2|}+\frac{1}{\varepsilon_1}\int d\mathbf{r}'\frac{\sigma_{pol}(\mathbf{r}',\mathbf{r}_2)}{|\mathbf{r}_1-\mathbf{r}'|}.\tag{A7}$$

The electrostatic potential calculated from Eq. (A7) is shown in Fig. 1 for the case of the source charge at the origin, as a function of $\mathbf{r}_1$.

We attribute the differences between Eqs. (A3) and (A7) to the fact that the type of electrostatic boundary conditions of our problem (Neumann-like) does not determine univocally the solution for the potential.[11] From this point of view, the calculation of the potential from the polarization charges can be though as a way of determinate the physically correct solution.

The full calculation of the exact electrostatic potential can now be accomplished using Eq. (A7). While this is in principle possible, it is extremely demanding from the numerical point of view, as for the calculation of the quantum dot electronic properties we need to perform integrations of the potential with respect to one or two three-dimensional arguments. On the other side, Eq. (A3) looks ideally suited for numerical calculations, as the three spatial directions are factorized in the integrand and then the integrals with the electronic wave functions (which in the strong-confinement approximation are also factorized), can be performed quite efficiently.

In consequence, we have adopted the following strategy for the numerical calculations: to use the potential as given by Eq. (A3), but correcting it by a function which is just the difference between Eqs. (A3) and (A7). Fortunately, this function turned out to be almost independent on the source or test coordinates; for instance, for $\Phi^{<}(\mathbf{r}_1,\mathbf{r}_2)$, the correction factor is accurately given by $0.89\varepsilon_r(\varepsilon_r-1)$.

In summary, instead of using Eqs. (A3), we will use its corrected version:

$$\Phi^{<}(\mathbf{r}_1,\mathbf{r}_2)=\frac{q}{\varepsilon_1 Q}\left(\frac{1}{\sqrt{\pi}}\int_0^{\infty}\frac{dt}{\sqrt{t}}\phi^{<}(\bar{x}_1,\bar{x}_2,t)\times\phi^{<}(\bar{y}_1,\bar{y}_2,t)\phi^{<}(\bar{z}_1,\bar{z}_2,t)+f(\mathbf{r}_1,\mathbf{r}_2)\right), \tag{A8}$$

where the ϕ functions are defined by Eq. (A4) and $f(\mathbf{r}_1,\mathbf{r}_2)$ is the correction function which brings $\Phi^{<}(\mathbf{r}_1,\mathbf{r}_2)$ equal to the exact value from Eq. (A7). As we indicate above, the correction function for coordinate values inside the dot is just a constant $f(\mathbf{r}_1,\mathbf{r}_2)\equiv C$, that nicely helps with the numerical calculations.

2. One-particle polarization self-energy

This contribution can be obtained from Eqs. (A8) and (A4) by taking $\mathbf{r}_1=\mathbf{r}_2=\mathbf{r}$, $q=-e_0$, excluding the real charge contribution ($l=m=n=0$) from the sums which define the integrating functions $\phi^{<}$, and dividing by 2 as corresponds to a self-energy. Accordingly,

$$V_s(\mathbf{r})=\frac{e_0^2}{2\varepsilon_1 Q}\left(\frac{1}{\sqrt{\pi}}\int_0^{\infty}\frac{dt}{\sqrt{t}}\phi^{<}(\bar{x},\bar{x},t)\times\phi^{<}(\bar{y},\bar{y},t)\phi^{<}(\bar{z},\bar{z},t)+C\right). \tag{A9}$$

Taking the expectation value of Eq. (A9) with the one-electron wave functions in the strong-confinement approximation

$$\psi_{k_xk_yk_z}(\mathbf{r})=\frac{1}{Q^{3/2}}\cos\left(\frac{\pi}{2}k_x\bar{x}-\alpha_x\right)\times\cos\left(\frac{\pi}{2}k_y\bar{y}-\alpha_y\right)\cos\left(\frac{\pi}{2}k_z\bar{z}-\alpha_z\right), \tag{A10}$$

where $k_x,k_y,k_z=1,2,\ldots,$ and $\alpha_j=\pi/2(0)$ when k_j is even (odd) ($j=x,y,z$) we obtain the associated polarization self-energy corrections

$$\Sigma^{CQD}(Q)\equiv\langle k_xk_yk_z|V_s(\mathbf{r})|k_xk_yk_z\rangle=\frac{e_0^2}{2\varepsilon_1 Q}\times\left(\frac{1}{\sqrt{\pi}}\int_0^{\infty}\frac{dt}{\sqrt{t}}I_{k_x}(t)I_{k_y}(t)I_{k_z}(t)+C\right). \tag{A11}$$

In the equation above,

$$I_{k_x}(t)=\sum_{l=-\infty}^{\infty}\xi^{|l|}\int_{-1}^{1}d\bar{x}e^{-t\{[1-(-1)^l]\bar{x}-2l\}^2}\cos^2\left(\frac{\pi k_x}{2}\bar{x}-\alpha_x\right), \tag{A12}$$

and equivalent expressions for $I_{k_y}(t)$ and $I_{k_z}(t)$. The ground-state self-energy correction is particularly simple, as $k_x=k_y=k_z=1,\alpha_x=\alpha_y=\alpha_z=0$, and then $I_{k_x}(t)=I_{k_y}(t)=I_{k_z}(t)=I_1(t)$ and

$$\Sigma^{CQD}(Q)=\frac{e_0^2}{2\varepsilon_1 Q}\left(\frac{1}{\sqrt{\pi}}\int_0^{\infty}\frac{dt}{\sqrt{t}}[I_1(t)]^3+C\right). \tag{A13}$$

We notice again that in Eqs. (A9), (A11), and (A13) the contribution of the real charge must be excluded.

3. Electron-donor impurity binding energy

The electron-donor impurity interaction potential can be obtained from Eqs. (A8) and (A4) by taking $\mathbf{r}_1=\mathbf{r}_e$, $\mathbf{r}_2=\mathbf{r}_i$ (the impurity coordinate), and $q=e_0$; accordingly,

$$V_c(\mathbf{r}_e,\mathbf{r}_i)=-\frac{e_0^2}{\varepsilon_1 Q}\left(\frac{1}{\sqrt{\pi}}\int_0^{\infty}\frac{dt}{\sqrt{t}}\phi^{<}(\bar{x}_e,\bar{x}_i,t)\times\phi^{<}(\bar{y}_e,\bar{y}_i,t)\phi^{<}(\bar{z}_e,\bar{z}_i,t)+C\right). \tag{A14}$$

For the study of the electron-donor impurity binding energy the following matrix elements should be calculated:

$$\langle k_xk_yk_z|-V_{c(\mathbf{r}_e,\mathbf{r}_i)}|k_x'k_y'k_z'\rangle=\frac{e_0^2}{\varepsilon_1 Q}\left(\frac{1}{\sqrt{\pi}}\int_0^{\infty}\frac{dt}{\sqrt{t}}J_{k_xk_x'}(\bar{x}_i,t)J_{k_yk_y'}(\bar{y}_i,t)J_{k_zk_z'}(\bar{z}_i,t)+C\right), \tag{A15}$$

where

$$J_{k_x k_x'}(\bar{x}_i,t)=\int_{-1}^{1} d\bar{x}_e \cos\left(\frac{\pi}{2}k_x\bar{x}_e-\alpha_x\right)$$
$$\times\cos\left(\frac{\pi}{2}k_x'\bar{x}_e-\alpha_x'\right)\phi^{<}(\bar{x}_e,\bar{x}_i,t), \tag{A16}$$

and equivalent expressions for $J_{k_y k_y'}$ and $J_{k_z k_z'}$. Eq. (A14) is valid if the impurity is located inside the dot. If the impurity is outside the dot, the one-dimensional potentials $\phi^{<}$ must be replaced by the one-dimensional potentials corresponding to the case where the impurity coordinate component takes values outside the dot.[21] Besides, C becomes a function of the impurity coordinate (but not of the electron coordinate) which we have determined numerically; this is the only case in our calculations where the correction function cannot be considered as a constant.

4. Electron-hole Coulomb energy

The electron-hole Coulomb potential is given by Eqs. (A8) and (A4) with $\mathbf{r}_1=\mathbf{r}_e$, $\mathbf{r}_2=\mathbf{r}_h$, and $q=e_0$,

$$V_c(\mathbf{r}_e,\mathbf{r}_h)=-\frac{e_0^2}{\varepsilon_1 Q}\left(\frac{1}{\sqrt{\pi}}\int_0^{\infty}\frac{dt}{\sqrt{t}}\phi^{<}(\bar{x}_e,\bar{x}_h,t)\right.$$
$$\left.\times\phi^{<}(\bar{y}_e,\bar{y}_h,t)\phi^{<}(\bar{z}_e,\bar{z}_h,t)+C\right). \tag{A17}$$

The electron-hole Coulomb energy for the ground-state exciton in a CQD is defined as

$$E_{Coul}^{CQD}(Q)=-\int d\mathbf{r}_e\int d\mathbf{r}_h|\Psi_{ex}^{CQD}(\mathbf{r}_e,\mathbf{r}_h)|^2 V_c(\mathbf{r}_e,\mathbf{r}_h), \tag{A18}$$

where

$$\Psi_{ex}^{CQD}(\mathbf{r}_e,\mathbf{r}_h)=\frac{1}{Q^3}\cos\left(\frac{\pi}{2}\bar{x}_e\right)\cos\left(\frac{\pi}{2}\bar{y}_e\right)\cos\left(\frac{\pi}{2}\bar{z}_e\right)$$
$$\times\cos\left(\frac{\pi}{2}\bar{x}_h\right)\cos\left(\frac{\pi}{2}\bar{y}_h\right)\cos\left(\frac{\pi}{2}\bar{z}_h\right) \tag{A19}$$

is the normalized ground-state exciton wave function of a CQD in the strong-confinement approximation. Replacing Eq. (A19) in Eq. (A18), we obtain

$$E_{Coul}^{CQD}(Q)=\frac{e_0^2}{\varepsilon_1 Q}\left\{\frac{1}{\sqrt{\pi}}\int_0^{\infty}\frac{dt}{\sqrt{t}}\left[\int_{-1}^{1}d\bar{x}_e\int_{-1}^{1}d\bar{x}_h\cos^2\left(\frac{\pi\bar{x}_e}{2}\right)\right.\right.$$
$$\left.\left.\times\cos^2\left(\frac{\pi\bar{x}_h}{2}\right)\phi^{<}(\bar{x}_e,\bar{x}_h,t)\right]^3+C\right\}. \tag{A20}$$

Defining two new integration variables $u=\bar{x}_e-\bar{x}_h$, and $v=\bar{x}_e+\bar{x}_h$, the v integral can be performed analytically and after some algebra the final expression for $E_{coul}^{CQD}(Q)$ is reduced to a twofold integral:

$$E_{coul}^{CQD}(Q)=\frac{e_0^2}{2\varepsilon_1 Q}\left(\sqrt{\pi}\int_0^{\infty}\frac{dt}{\sqrt{t}}[K(t)]^3+C\right), \tag{A21}$$

with

$$K(t)=\sum_{l=-\infty}^{\infty}\xi^{|l|}\int_0^1 du e^{-t\pi^2(u-l)^2}$$
$$\times\left((1-u)[2+\cos(2\pi u)]+\frac{3}{2\pi}\sin(2\pi u)\right). \tag{A22}$$

In the absence of dielectric mismatch, $\xi=0$ and then only the term $l=0$ from Eq. (A22) gives a finite nonzero contribution.[17] It is interesting to note that our procedure for the calculation of E_{Coul}^{CQD} reduces the original ninefold integration of Eqs. (A18) and (A7) to the twofold integration of Eqs. (A21) and (A22).

*Permanent address: Facultad de Formación Docente en Ciencias y Facultad de Ingeniería Química, Universidad Nacional del Litoral (UNL), Santiago del Estero 2829, 3000 Santa Fe, Argentina.

[1] A. D. Yoffe, Adv. Phys. **42**, 173 (1993).
[2] L. Banyai and S. W. Koch, in *Semiconductor Quantum Dots* (World Scientific, Singapore, 1993).
[3] U. Woggon and S. V. Gaponenko, Phys. Status Solidi B **189**, 285 (1995).
[4] A. P. Alivisatos, MRS Bull. **23**, 18 (1998); A. J. Nozik and O. I. Mićić, *ibid.* **23**, 24 (1998).
[5] J. Y. Marzin, J. M. Gérard, A. Izrael, D. Barrier, and G. Bastard, Phys. Rev. Lett. **73**, 716 (1994).
[6] W. Wegscheider, G. Schedelbeck, G. Abstreiter, M. Rother, and M. Bichler, Phys. Rev. Lett. **79**, 1917 (1997).
[7] Ph. Lelong and G. Bastard, Solid State Commun. **98**, 819 (1996).
[8] L. E. Brus, J. Chem. Phys. **79**, 5566 (1983); **80**, 4403 (1984).
[9] Al. L. Efros and A. L. Efros, Sov. Phys. Semicond. **16**, 772 (1982).
[10] G. Bastard, in *Wave Mechanics Applied to Semiconductor Heterostructures* (Les Editions de Physique, Les Ulis, Cedex, 1988).
[11] J. D. Jackson, *Classical Electromagnetism* (Wiley, New York, 1962).
[12] J. M. Ferreyra and C. R. Proetto, Phys. Rev. B **52**, R2309 (1995); C. R. Proetto, Phys. Rev. Lett. **76**, 2824 (1996).
[13] M. Lannoo, C. Delarue, and G. Allan, Phys. Rev. Lett. **74**, 3415 (1995); G. Allan, C. Delarue, M. Lannoo, and E. Martin, Phys. Rev. B **52**, 11 982 (1995).
[14] R. Tsu and D. Babić, Appl. Phys. Lett. **64**, 1806 (1994).

[15] *Functions*, edited by M. Abramovitz and I. A. Stegun, *Handbook of Mathematical Functions* (Dover, New York, 1970).
[16] Q. Y. Ye, R. Tsu, and E. H. Nicollian, Phys. Rev. B **44**, 1806 (1991).
[17] G. Fishman, R. Romestain, and J. C. Vial, J. Phys. IV **3**, 355 (1993); R. Romestain and G. Fishman, Phys. Rev. B **49**, 1774 (1994).
[18] D. Babić, R. Tsu, and R. F. Greene, Phys. Rev. B **45**, 14 150 (1992).
[19] H. van Houten, C. W. J. Beenaker, and A. M. Staring, in *Single Charge Tunneling*, edited by H. Grabert and M. Devoret (Plenum, New York, 1992).
[20] T. Takagahara Phys. Rev. B **47**, 4569 (1993).
[21] M. Kumagai and T. Takagahara, Phys. Rev. B **40**, 12 359 (1989).